Wind turbines convert wind energy to electricity for distribution. Conventional horizontal axis turbines can be divided into three components:

- The rotor component, which is approximately 20% of the wind turbine cost, includes the blades for converting wind energy to low speed rotational energy.
- The generator component, which is approximately 34% of the wind turbine cost, includes the electrical generator, the control electronics, and most likely a gearbox (e.g. planetary gearbox,[28] adjustable-speed drive[29] or continuously variable transmission[30]) component for converting the low speed incoming rotation to high speed rotation suitable for generating electricity.
- The structural support component, which is approximately 15% of the wind turbine cost, includes the tower and rotor yaw mechanism.[31]

A 1.5 MW wind turbine of a type frequently seen in the United States has a tower 80 metres (260 ft) high. The rotor assembly (blades and hub) weighs 48,000 pounds (22,000 kg). The nacelle, which contains the generator component, weighs 115,000 pounds (52,000 kg). The concrete base for the tower is constructed using 58,000 pounds (26,000 kg) of reinforcing steel and contains 250 cubic yards (190 m^3) of concrete. The base is 50 ft (15 m) in diameter and 8 ft (2.4 m) thick near the center.[32]

Components of a horizontal-axis wind turbine

Size comparison of a five-year-old child with an Enercon E-70 wind turbine rotor hub on El Hierro, Canary Islands.

Unconventional designs

Main article: Unconventional wind turbines

One E-66 wind turbine at Windpark Holtriem, Germany, carries an observation deck, open for visitors. Another turbine of the same type, with an observation deck, is located in Swaffham, England. Airborne wind turbines have been investigated many times but have yet to produce significant energy. Conceptually, wind turbines may also be used in conjunction with a large vertical solar updraft tower to extract the energy due to air heated by the sun.

Wind turbines which utilise the Magnus effect have been developed.[33]

The ram air turbine is a specialist form of small turbine that is fitted to some aircraft. When deployed, the RAT is spun by the airstream going past the aircraft and can provide power for the most essential systems if there is a loss of all on–board electrical power.[citation needed]

The corkscrew shaped wind turbine at Progressive Field in Cleveland, Ohio
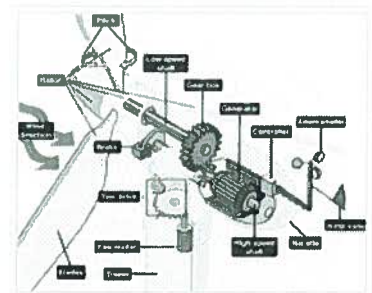
Small wind turbines

Main article: Small wind turbine

Small wind turbines may be used for a variety of applications including on- or off-grid residences, telecom towers, offshore platforms, rural schools and clinics, remote monitoring and other purposes that require energy where there is no electric grid, or where the grid is unstable. Small wind turbines may be as small as a fifty-watt generator for boat or caravan use. The U.S. Department of Energy's National Renewable Energy Laboratory (NREL) defines small wind turbines as those smaller than or equal to 100 kilowatts.[34] Small units often have direct drive generators, direct current output, aeroelastic blades, lifetime bearings and use a vane to point into the wind.
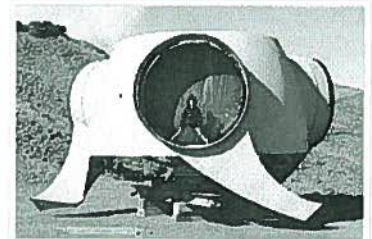
Larger, more costly turbines generally have geared power trains, alternating current output, flaps and are actively pointed into the wind. Direct drive generators and aeroelastic blades for large wind turbines are being researched.
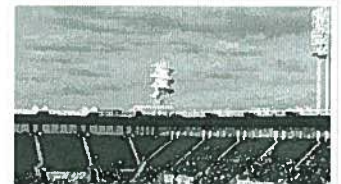
Wind turbine spacing

On most horizontal windturbine farms, a spacing of about 6-10 times the rotor diameter is often upheld. However, for large wind farms distances of about 15 rotor diameters should be more economically optimal, taking into account typical wind turbine and land costs. This conclusion has been reached by research[35] conducted by Charles Meneveau of the Johns Hopkins University,[36]

A small Quietrevolution QR5 Gorlov type vertical axis wind turbine in Bristol, England. Measuring 3m in diameter and 5m high, it has a nameplate rating of 6.5kW to the grid.

and Johan Meyers of Leuven University in Belgium, based on computer simulations[37] that take into account the detailed interactions among wind turbines (wakes) as well as with the entire turbulent atmospheric boundary layer. Moreover, recent research by John Dabiri of Caltech suggests that vertical wind turbines may be placed much more closely together so long as an alternating pattern of rotation is created allowing blades of neighbouring turbines to move in the same direction as they approach one another.[38]

Accidents

Several cases occurred where the housings of wind turbines caught fire. As housings are normally out of the range of standard fire extinguishing equipment, it is nearly impossible to extinguish such fires on older turbine units which lack fire suppression systems. In several cases one or more blades were damaged or torn away.[39] In 2010 70 mph (110 km/h; 61 kn) storm winds damaged some blades, prompting blade removal and inspection of all 25 wind turbines in Campo Indian Reservation in the US State of California. [40] Several wind turbines also collapsed.

Place	Date	Type	Nacelle height	Rotor dia.	Year built	Reason	Damage and casualties
Ellenstedt, Germany	October 19, 2002					[41]	
Schneebergerhof, Germany	December 20, 2003	Vestas V80		80 m		[41]	
Wasco, Oregon, USA	August 25, 2007	Siemens				Human error: turbine restarted while blades were locked in maximum wind-resistance mode[42]	1 worker killed, 1 injured
Stobart Mill, UK	December 30, 2007	Vestas			1982	[43]	
Hornslet, Denmark	February 22, 2008	Nordtank NKT 600-180	44.5 m	43 m	1996	Brake failure[44][45]	
Searsburg, Vermont, USA	October 16, 2008	Zond Z-P40-FS			1997	Rotor blade collided with tower during strong wind and destroyed it[46]	
Altona, New York, USA	March 6, 2009	GE Energy 1.5MW[47]				Lightning likely [48]	
Fenner, New York, USA	December 27, 2009	GE Energy 1.5 MW [citation needed]				[49]	
Kirtorf, Germany	June 19, 2011	DeWind D-6	68.5 m	62 m	2001		
Ayrshire, Scotland	December 8, 2011	Vestas V80 2MW[50]				[51]	

Records

Largest capacity
: The Enercon E-126 has a rated capacity of 7.58 MW,[52] has an overall height of 198 m (650 ft), a diameter of 126 m (413 ft), and is the world's largest-capacity wind turbine since its introduction in 2007.[53] At least five companies are working on the development of a 10MW turbine.

Largest swept area
: The turbine with the largest swept area is the Siemens SWT-6.0-154, with a diameter of 154 m, giving a total sweep of 18,600 m²[54][55]

Tallest
: The tallest wind turbines are two standing in Paproć, Poland, 210 meters tall, also constructed by Fuhrlaender in late 2012. Their axis have the same height as previous tallest turbine,
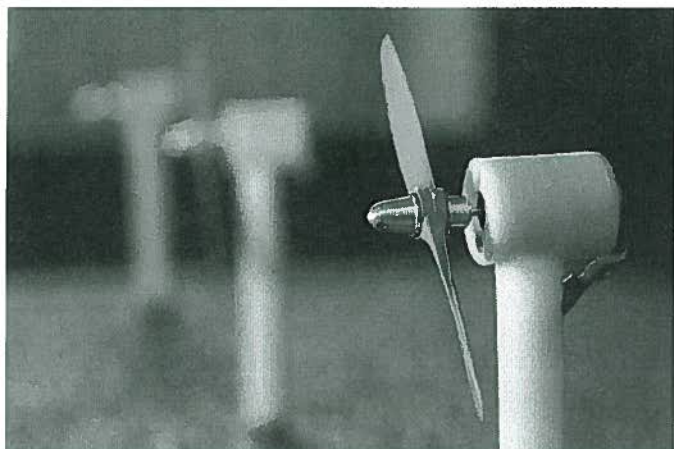
THE JHU GAZETTE

January 18, 2011

New study yields better turbine spacing for large wind farms

Research seeks cleaner, more cost-efficient energy

By Phil Sneiderman, *Homewood*

A wind tunnel on the Homewood campus allows researchers to experiment with variables such as the correct spacing of wind turbines. Charles Meneveau and a colleague have devised a new formula for determining the optimal positioning. Photo: Will Kirk/Homewoodphoto.jhu.edu

Large wind farms are being built around the world as a cleaner way to generate electricity, but operators are still searching for the most cost-effective and efficient way to arrange the massive turbines that turn moving air into power.

To help steer wind farm owners in the right direction, Charles Meneveau, a Johns Hopkins fluid mechanics and turbulence expert, working with a colleague in Belgium, has devised a new formula through which the optimal spacing for a large array of turbines can be obtained.

"I believe our results are quite robust," said Meneveau, who is the Louis Sardella Professor of Mechanical Engineering in the university's Whiting School of Engineering. "They indicate that large wind farm operators are going to have to space their turbines farther apart."

The newest wind farms, which can be located on land or offshore, typically use turbines with rotor diameters of about 300 feet. Currently, turbines on these large wind farms are typically spaced about seven rotor diameters apart. The new spacing model developed by Meneveau and Johan Meyers, an assistant professor at Katholieke Universiteit Leuven in Belgium, suggests that placing the wind turbines 15 rotor diameters apart—more than twice as far apart as in the current layouts—results in more cost-efficient power generation.

The study by Meneveau and Meyers was presented recently at a meeting of the American Physical Society Division of Fluid Dynamics.

The research is important because large wind farms—consisting of hundreds or even thousands of turbines—are planned or already operating in the western United States, Europe and China. "The early experience is that they are producing less power than expected," Meneveau said. "Some of these projects are underperforming."

Earlier computational models for large wind farm layouts were based on simply adding up what happens in the wakes of single wind turbines, Meneveau said. The new spacing model, he said, takes into account interaction of arrays of turbines with the entire atmospheric wind flow.

Meneveau and Meyers argue that the energy generated in a large wind farm has less to do with horizontal winds and is more dependent on the strong winds that the turbulence created by the tall turbines pulls down from higher up in the atmosphere. Using insights gleaned from high-performance computer simulations as well as from wind tunnel experiments, they determined that in the correct spacing, the turbines alter the landscape in a way that creates turbulence, which stirs the air and helps draw more powerful kinetic energy from higher altitudes.

The experiments were conducted in the university's wind tunnel, located on the Homewood campus, which uses a large fan to generate a stream of air. Before it enters the testing area, the air passes through an "active grid," a curtain of perforated plates that rotate randomly and create turbulence so that the air moving through the tunnel more closely resembles real-life wind conditions.

Air currents in the tunnel pass through a series of small three-bladed model wind turbines mounted atop posts, mimicking an array of full-size wind turbines. Data concerning the interaction of the air currents and the model turbines is collected by using a measurement technique called stereo particle-image-velocimetry, which requires a pair of high-resolution digital cameras, smoke and laser pulses.

Further research is needed, Meneveau said, to learn how varying temperatures can affect the generation of power on large wind farms. He has applied for continued funding to conduct such studies.

Optimal turbine spacing in fully developed wind-farm boundary layers

Johan Meyers[1] and Charles Meneveau[2]

[1]Department of Mechanical Engineering, Katholieke Universiteit Leuven,

Celestijnenlaan 300A — bus 2421, B3001 Leuven, Belgium

[2]Department of Mechanical Engineering & Center for Environmental and

Applied Fluid Mechanics, Johns Hopkins University,

3400 North Charles Street, Baltimore MD 21218, USA

February 11, 2011

Abstract

As wind farms become larger, the asymptotic limit of the "fully developed", or "infinite", wind farm has been receiving increased interest. This limit is relevant for wind farms on flat terrain whose length exceeds the height of the atmospheric boundary layer by over an order of magnitude. Recent computational studies based on Large Eddy Simulation have identified various mean velocity equilibrium layers, and have led to parameterizations of the effective roughness height that allow predicting the wind velocity at hub-height as function of parameters such as wind turbine spacing and loading factors. In the current paper, we employ this as a tool to make predictions of optimal wind turbine spacing as function of these parameters, as well as in terms of the ratio of turbine costs to land-surface costs. For realistic cost ratios, we find that the optimal average turbine spacing may be considerably higher than conventionally used in current wind-farm implementations.

Keywords: wind farm, wind energy, optimal wind turbine spacing, large-eddy simulation

1. INTRODUCTION

Recently, wind energy has received renewed interest. This originates in part from large funding programs by American and European governments, and comes from the realization that wind energy will be an important contributor in the production of affordable and clean energy in the next decades. In various scenarios,[1,2] a contribution of wind energy to the overall electricity production up to 20% is aimed at by 2030. To realize these targets, larger wind farms (both on- and off-shore), covering increasingly larger surface areas are required. When large-scale wind-farm implementations are considered, the total drag induced by all turbines in the farm may change the equilibrium in the atmospheric surface layer. In particular, with a characteristic height of the ABL of about 1 km, wind farms with horizontal extents exceeding 10–20 km may therefore approach the asymptotic limit of "infinite" wind farms, and the boundary layer flow may approach a new fully developed regime, which depends on the additional surface drag induced by the wind farm. In the current study, we focus

on this asymptotic "infinite" wind-farm regime, and investigate the optimal wind-turbine spacing in these wind farms to either optimize the ratio of total power output per land surface, or the ratio of total power output per unit of total cost that also includes cost of turbines. Depending on the ratio between total costs per turbine and total costs per land surface, in the case of "infinite" wind farms, we find that the optimal average turbine spacing may be considerably higher then conventionally used in current wind-farm implementations.

Design and optimization of single wind turbines is well explored nowadays, often using blade-element–momentum theory, and Glauert's theory for rotor aerodynamics.[3,4] Also effects of turbine wake aerodynamics have received much attention.[5] Studies of the interaction of large wind farms and the atmospheric boundary layer (ABL) are far less prevalent. In this area, pioneering work was performed by Frandsen,[6] who formulated a model for the surface roughness induced by "infinite" wind turbine arrays. More recently, the subject gained renewed interest in the context of off-shore wind-farm under performance.[7] Very recently, studies employed large-eddy simulations to study wind-farm–ABL interactions,[8,9] focusing on the 'infinite' wind-farm limit. Moreover, in Ref. 8, Frandsen's model for the induced wind-farm surface roughness was refined, to include effects of turbine-wake mixing.

When turbine spacing is considered in a more conventional approach, minimum wind-turbine spacing in wind farms is mainly governed by the desire to limit wake-induced fatigue loads in turbines located downstream of a prior row of turbines.[5] However, large wind farms increase the effective surface roughness experienced by the ABL,[6,8] such that the effective wind velocity at turbine-hub height decreases compared to an unloaded ABL. Hence, increasing the installed power per land surface area (i.e. decreasing the average wind-turbine spacing) has an inverse effect on the total extracted power per turbine. Depending on the cost per turbine, and the cost of land used for wind farms, this leads to an optimization problem for wind-turbine spacing in wind farms, where the optimal spacing is given by economical constraints. In the current work the refined effective roughness model of Ref. 8 is used as the basis to elaborate a model for overall wind-farm power output per land surface, taking fully developed wind-farm–ABL interactions into account. A detailed discussion is presented on optimal turbine spacing, and its dependence on economical parameter, and operating regimes.

Wind-turbine operation is often classified into three regions: region I–III.[4,10] The first region is at very low wind speeds where aerodynamic forces cannot overcome the turbine's internal friction losses. At very high wind speeds (Region III), the power output of turbines is restricted by loading constraints on its mechanical structures and by economical constraints on the size of the power generator. In this region, turbine power is controlled at a constant level, independent of wind speed, either by stalling the turbine blades, or by feathering the turbine.[4] In region II, power output is not restricted, and wind turbines work close to their aerodynamical optimal operating conditions. In the current work, we focus in large part on optimization of turbine-spacing in region II, where turbine thrust and power coefficients are close to optimal. At the end of Section 3, region III operation and its influence on optimal turbine spacing in wind farms, is discussed. It will be argued that feathering may have an impact on the optimal turbine spacing in the equilibrium wind-farm ABL, while stalling the turbine keeps the optimal spacing at the region-II optimum.

The paper is further organized as follows. First, in Section 2, the model for wind-farm optimization is elaborated. In Section 3, optimization results are presented and discussed. Finally, conclusions are presented in Section 4.

2. MODEL FOR WIND-FARM OPTIMIZATION

First, some definitions and conventions for wind-turbine thrust and power, which will be further used in the current study, are introduced in §2.1. Next, in §2.2, standard relations for the atmospheric

2

boundary layer are briefly reviewed. Subsequently, the induced surface-roughness model for wind farms[8] is discussed in §2.3. Finally, in §2.4 the wind-farm optimization problem is defined in terms of normalized farm power.

2.1. Definitions and conventions

In conventional wind-turbine momentum theory, the thrust of a single wind-turbine on the surrounding flow is expressed as

$$F_T = -\frac{1}{2}C_T\rho U_\infty^2 A, \tag{1}$$

with C_T the thrust coefficient, U_∞ the upstream undisturbed flow velocity at hub height, and $A = \pi D^2/4$ the turbine-rotor area (with D the rotor diameter). However, for large wind-turbine arrays with significant interactions among wind turbines and wakes, this reference velocity U_∞ is not readily known and would require arbitrary decisions about what upstream distance to use when specifying the velocity. Moreover, such a reference velocity would depend on farm parameters such as the average turbine spacing, and turbine loading. Instead, for wind farms, it is useful to base the relations for thrust on the prevailing axial velocity at the rotor-disk position, U_d, such that

$$F_T = -\frac{1}{2}C_T'\rho U_d^2 A. \tag{2}$$

Note that the value of C_T' is straightforwardly related to the lift and drag coefficients of the turbine blades (see e.g. Ref. 9 for an elaboration), and much less sensitive to farm parameters such as average turbine spacing. Moreover, in large-eddy simulations of wind farms,[8] U_d is readily available during the simulation, such that Eq. (2) can be directly employed as a force model.

For a lone-standing turbine, it is possible to relate C_T' to C_T by using classic actuator disk theory. This allows us to express

$$U_d = U_\infty(1 - a), \quad C_T' = \frac{C_T}{(1-a)^2}, \tag{3}$$

with a the axial induction factor.[9] For the Betz limit[4] (i.e., $C_T = 8/9$, and $a = 1/3$), we obtain $C_T' = 2$. Using typical values $C_T = 0.75$, and $a = 1/4$ (which have been used before for modeling wind turbines)[11] leads to $C_T' = 4/3$. Obviously, for wind farms, Eq. (3) is not valid, though the typical values for C_T' remain applicable.

For wind-turbine farms, it is further useful to express the thrust in relation to the average land surface area S per turbine ($S = \ell_x\ell_y$, with ℓ_x, ℓ_y the average turbine-spacing in stream-wise and span-wise directions), leading to

$$F_T = \frac{1}{2}c_{ft}'\rho U_d^2 S, \tag{4}$$

with a friction coefficient c_{ft}' based on the horizontal surface rather than frontal area. Further,

$$c_{ft}' = \frac{\pi C_T'}{4s_x s_y} = \frac{\pi C_T'}{4s^2}, \tag{5}$$

with $s_x = \ell_x/D$, $s_y = \ell_y/D$, and $s = \sqrt{s_x s_y}$.

The power extracted on average by wind turbines from the atmospheric boundary layer corresponds to

$$P = \frac{1}{2}C_T'\rho U_d^3 A = \frac{1}{2}c_{ft}'\rho U_d^3 S. \tag{6}$$

This is not equivalent to the power P_{ax} on the turbine axis. The latter relates to the torque and rotational velocity of the turbine. The drag forces on the turbine blades increase thrust, but reduce torque. From

3

an energetic point of view, the drag forces lead to losses, corresponding to a conversion of mean-flow energy in the atmospheric boundary layer into turbulent motion and heat. Using the power coefficient C_P, and C_P' (respectively with respect to U_∞, and U_d), the power on the turbine axis corresponds to

$$P_{ax} = P\frac{C_P'}{C_T'} = P\frac{C_P}{C_T(1-a)} \tag{7}$$

Using actuator disk theory, it is straightforward to find that $C_P = C_P'(1-a)^3$. For the Betz limit (i.e., $C_P = 16/27$, and $a = 1/3$), $C_P' = 2.0$.

For wind turbines, typical optimal values may be $C_P \approx 0.34$ and $a \approx 1/4$, such that $C_P' \approx 0.8$, and $P_{ax} \approx 0.6P$. In reality, the ratio C_P'/C_T' depends on the turbine working region. In region II, C_P'/C_T' is close to optimal, with high values for C_T', and C_P'. Consequently, in this operating region, optimization to P or P_{ax} is roughly equivalent. In region III, the turbine's power output is controlled to be constant. Depending on the control mechanism, this may lead to a large decrease in C_P'/C_T'. Consequences of region III operation on the optimization results in the current work are addressed, separately, at the end of Section 3. Until then, we assume $P \sim P_{ax}$, and formulate the wind-farm–ABL optimization problem in terms of P.

2.2. Geostrophic wind and ABL relations

In the current subsection, we briefly review classical relations for the atmospheric boundary layer, as, e.g., well documented in Ref. 12.

In the atmospheric boundary layer (ABL), the driving force is the geostrophic wind, of velocity magnitude G, on top of the ABL, which is given by geostrophic balance condition without the effects of friction. Inside the boundary layer, a balance exists between pressure forces, Reynolds stresses, and Coriolis forces induced by the Earth's rotation. Since the velocity in the ABL decreases towards the surface, Coriolis forces also decrease, which causes the velocity to turn away from the geostrophic wind direction at lower altitudes, often referred to as the Ekman spiral. Conventionally, a reference frame is selected which is aligned with the wind speed near the surface (in the inner layer of the boundary layer). In this case, the geostrophic wind G is defined with two components, i.e. U_G in stream-wise, and V_G in span-wise direction, such that $G = (U_G^2 + V_G^2)^{1/2}$, and $\gamma = \arctan(-V_G/U_G)$ the angle between the geostrophic wind direction, and the wind direction near the surface. Classical similarity theory then leads to[12]

$$\frac{U_G}{u_*} = \frac{1}{\kappa}\ln\left(\frac{u_*}{f z_0}\right) - C, \tag{8}$$

$$\frac{V_G}{u_*} = -A \tag{9}$$

with $\kappa = 0.4$ the Von Kármán constant, and where $C \approx 4.5$, and $A \approx 11.25$ are found to be good values.[6] Further, z_0 is the surface roughness. In the context of wind-farms, this is related to total roughness induced by the ground surface and the wind turbines on the ABL. Likewise, u_* is the friction velocity, which is related to the total friction exerted by the ground and wind turbines on the boundary layer. Further details on z_0, and u_*, and their relation to the wind-farm parametrization, etc., are provided in §2.3. Finally,

$$f = 2\Omega \sin\phi \tag{10}$$

is the Coriolis parameter. For $\Omega = 2\pi/(24 \times 3600\ s) = 7.27 \times 10^{-5}$ 1/s, and, e.g., at 40 degree latitude, we get $f = 9.34 \times 10^{-5}$ 1/s.
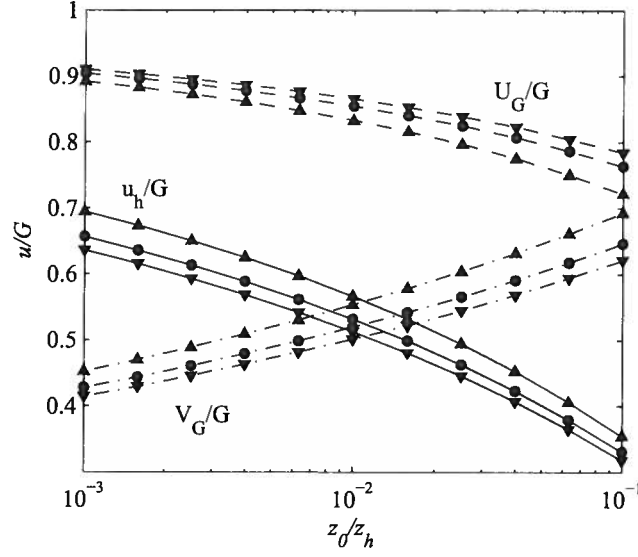
4

Figure 1: Relation between geostrophic wind and wind speed at turbine hub height as function of the surface roughness in the ABL (cf. Eqs.(8,9,11) with $f = 9.34 \times 10^{-5}$1/s, and $z_h = 100$m). (—): u_h/G; (– –): U_G/G; and (–·): V_G/G. (▲): $Ro_h = 1000$; (●): $Ro_h = 2000$; and (▼): $Ro_h = 3000$;

Combining Eq. (8), and (9), leads to

$$\frac{G}{u_*} = \sqrt{A^2 + \left[\frac{1}{\kappa}\ln\left(\frac{u_*}{G}Ro\right) - C\right]^2}, \tag{11}$$

where the dimensionless group $Ro = G/(fz_0)$ has the form of a Rossby number, expressing a ratio between inertia and Coriolis forces. In the current work, we are mainly interested in the reaction of the ABL to changes in the surface roughness induced by wind turbines. Therefore, we introduce an alternative Rossby number, using the turbine hub-height as reference length scale, such that

$$Ro_h = \frac{G}{fz_h} = Ro\frac{z_0}{z_h}, \tag{12}$$

and we will evaluate the effect of variations in z_0/z_h, while keeping Ro_h constant. A representative reference value for Ro_h may, e.g., be estimated using $f = 9.34 \times 10^{-5}$ 1/s, $G = 20$m/s, and $z_h = 100$m, leading to $Ro_h \approx 2140$.

Using expression (11), it is useful to investigate the relation between the geostrophic velocity G, and u_h, the mean streamwise velocity at turbine hub-height, which we estimate here using Monin-Obukhov similarity under neutral stratification conditions (the log-law for rough walls). One can write $u_h \approx u^*/\kappa \ln(z_h/z_0)$, with z_h the turbine-hub height. To this end, G/u_* is solved numerically from Eq. (11), using MATLAB's fsolve function. Alternatively, fits to the inverse function may be employed, as, e.g., proposed in Ref. 7 and further explored in the Appendix, where such an approximate expression is given explicitly (since it involves errors on the order of 7% for G/u_*, here we continue to use the numerical solution). In Figure 1, u_h/G is displayed, together with the separate geostrophic components U_G/G, and V_G/G as function of the surface roughness z_0 (with z_0 covering a range between 0.1m and 10m – as may be encountered in large wind farms[8] – normalized by $z_h = 100$). In the figure, three different values of Ro_h are displayed, i.e. $Ro_h = 1000$, $Ro_h = 2000$, and $Ro_h = 3000$.

5

It is appreciated that u_h/G drops significantly when the surface roughness z_0 increases, reducing the available wind speed at hub height. Figure 1 also illustrates that the angle between the geostrophic wind direction, and the surface wind direction increases when z_0 increases, as is apparent from the changes in U_G/G, and V_G/G. The induced roughness z_0 in a wind farms strongly depends on the average turbine spacing s, and the thrust coefficient C_T'. Hence, since the geostrophic wind G is the driving force in the ABL, the strong dependence of u_h/G on z_0 should be taken into account when wind-farm lay-out for optimal power output is considered. This is addressed in the next section. For this analysis to follow, we will keep the Rossby number Ro_h constant at 2000.

2.3. Wind-farm induced surface roughness from LES

Depending on atmospheric conditions, the magnitude of the geostrophic wind, and surface roughness, the height H of the atmospheric boundary layer typically is of the order of 1–2km. Consequently, wind turbines, with a typical hub height of 100m are situated within the ABL's inner region ($\leq 0.1H$). In the classical view on boundary layers, 'outer-layer' and 'inner-layer' dynamics are presumed to be independent (see, e.g., Ref. 13), and the inner layer dynamics are characterized by the surface roughness z_0, and the friction velocity (characterizing the overall wall friction). In the context of wind farms, Fransden[6] formulated a model for the surface roughness induced by the farm.

Based on a suite of large-eddy simulation cases, this model was recently refined, including effects of turbine-wake mixing in the formulation.[8] Specifically, the simulations used periodic boundary conditions in horizontal planes to represent fully developed conditions relevant to wind farms that are 10-20 times longer than the ABL height. For illustration, figure 2 shows contours of streamwise velocity on three perpendicular planes across a snapshot of the flow. Domains containing, e.g. 6×8 wind turbines were used. The wind turbines were represented using the 'drag-disk' model. In a recent detailed validation study[14] it was demonstrated that, except for near-wake effects close to the turbines with $x \leq 3D$, these models allow an accurate representation of the overall wake structures behind turbines. Moreover, also Reynolds stresses, which are responsible for the main vertical fluxes of energy towards the wind turbines,[8,15] were found to be accurately predicted,[14] thus allowing an accurate representation of the interaction of the wind farms with the atmospheric boundary layer.

The flow was forced using a streamwise pressure gradient (instead of Coriolis forcing) with the understanding that the 'outer forcing' method should not significantly affect the 'inner-layer' structure of the flow, i.e. the relationship between the resulting roughness and, e.g. the hub-height z_h. As can be seen in Fig. 2, the wakes meander back and forth before interacting with the next wind turbine row. Also, in the vertical direction, large-scale structures mix the fluid momentum thus entraining kinetic energy into the region where the wind turbines are located. As discussed in detail in Refs. 8, 15, such vertical entrainment is a crucial mechanism in the limit of infinite wind farms.

The suite of LES were processed to obtain horizontally averaged streamwise velocity profiles. As a confirmation of an important assumption made in the original Frandsen (1992)[6] model, the simulations showed that in the inner layer of a fully developed wind-turbine atmospheric boundary layer, two equilibrium (log) layers exist. The first equilibrium layer, the 'high' layer, is situated above the wind turbine canopy, with a friction velocity u_{*hi} ("high" denoted by subscript 'hi'). This friction velocity is associated with the total friction induced by the ground surface and the wind turbines, balancing the driving forces in the ABL. At very high Reynolds number, it can also be expected that $u_{*hi} \approx (-\langle \overline{u'w'} \rangle_z)^{1/2}$ (with $-\langle \overline{u'w'} \rangle_z$ the Reynolds stresses at a height z, with $H \gg z \gtrsim z_h$). A second "low" layer exists below the wind turbine array ("low" denoted by subscript 'lo'), where the friction velocity is reduced due to the momentum lost to the wind-turbines, and equals $u_{*lo} = \sqrt{\tau_w/\rho}$, where τ_w is the stress at the ground. A new observation was made based on the LES results, namely of a third layer separating the two log-layers, namely a wake-mixing region at turbine hub height.[8]
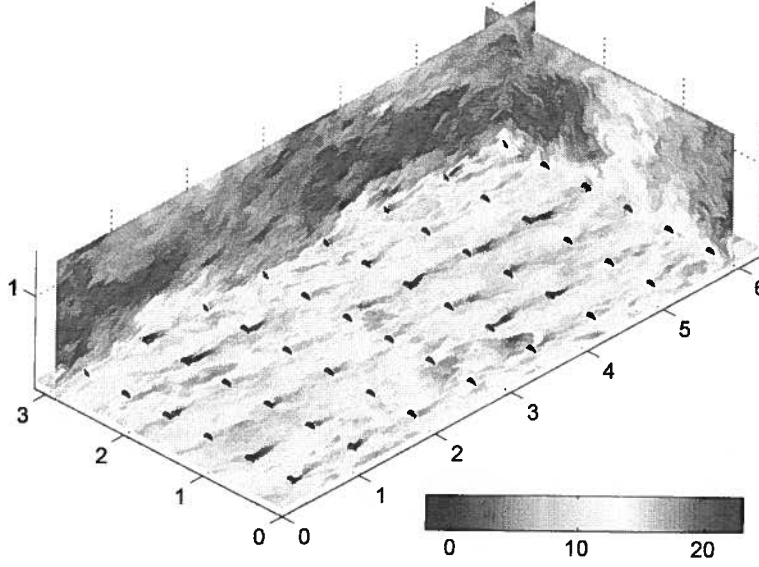
Figure 2: Contours of streamwise velocity (in units of u_{*hi}) on three orthogonal planes across the domain, obtained from LES.[8] The horizontal plane cuts the wind turbine rotor planes at hub-height. The model for effective roughness height associated to large wind farms was developed using a suite of such LES under various geometric and loading conditions.[8]

Using the insights from the LES, in Ref. 8, a new model was proposed for the ratio u_{*lo}/u_{*hi}, by modifying Frandsen's original model[6] to include effects of the wake making in the third layer. The ratio between the friction velocities corresponds to[8]

$$\frac{u_{*lo}}{u_{*hi}} = \frac{\ln\left[\frac{z_h}{z_{0,hi}}\left(1 + \frac{D}{2z_h}\right)^{\frac{v_w^*}{1+v_w^*}}\right]}{\ln\left[\frac{z_h}{z_{0,lo}}\left(1 - \frac{D}{2z_h}\right)^{\frac{v_w^*}{1+v_w^*}}\right]},$$ (13)

where $z_{0,hi}$ is the surface roughness induced by the wind farm, and v_w^* is a normalized "augmented wake eddy viscosity", estimated as[8]

$$v_w^* \approx 28\sqrt{c_{ft}/2},$$ (14)

with $c_{ft} = \pi C_T/4s^2$. This normalized eddy viscosity corresponds to the extra eddy viscosity introduced by the turbine wakes in the ABL, normalized with the boundary layer eddy-viscosity $\kappa u_* z$, in absence of turbines.[8] In the surface-roughness model introduced in Ref. 8, it follows from an eddy viscosity formulation which is used to estimate the logarithmic slope of the mean velocity profile at turbine hub height, connecting the "low" and "high" equilibrium layers. Typical values for v_w^* obtained from large-eddy simulations in Ref. 8 range from 0.5 to 3.5.

Similar to the friction velocities, a high surface roughness $z_{0,hi}$, and a low surface roughness $z_{0,lo}$ are respectively associated to the upper and lower equilibrium layer. The 'low' surface roughness $z_{0,lo}$ is the standard roughness associated with the land surface length-scales on which the wind farm is build. The high surface roughness, is the surface roughness felt by the equilibrium layer above the

turbines. In the new model, it is given by[8]

$$\frac{z_{0,hi}}{z_h} = \left(1 + \frac{D}{2z_h}\right)^{\frac{\nu_w^*}{1+\nu_w^*}} \exp\left(-\left[\frac{c_{ft}}{2\kappa^2} + \left(\ln\left[\frac{z_h}{z_{0,lo}}\left(1 - \frac{D}{2z_h}\right)^{\frac{\nu_w^*}{1+\nu_w^*}}\right]\right)^{-2}\right]^{-1/2}\right).$$ (15)

Using the wind-farm induced surface roughness $z_{0,hi}$, and the relations presented in §2.2 (and replacing z_0 with $z_{0,hi}$) we are able to evaluate the effect of wind farms on the ABL. To this end, we rely in the current study on formulations using c_{ft}' (cf. §2.1, and next subsection), while in the model proposed by Calaf $et\ al.$, c_{ft} is used. In the context of wind farms, the relation between both is not necessarily straightforward, as discussed in §2.1. Here, we will use the strong approximation that $c_{ft} \approx 9/16 c_{ft}'$, i.e. using Eq. (3), with $a = 1/4$.

In terms of the geostrophic wind and ABL relations introduced in §2.2, it is $z_{0,hi}$, and u_{*hi}, which are important. These are respectively the roughness height and friction velocity experienced by the ABL above the wind farm. Hence, u_*, and z_0 in Eqs. (8)–(9), and (11)–(12) should be replaced by $z_{0,hi}$, and u_{*hi} in the context of wind farms.

2.4. Normalized farm power and optimization problem

We now turn to the optimization problem. We focus on the normalized farm power, which serves as a basis for the definition of the cost function in the optimization. The power output normalized using the geostrophic wind G, and per unit land surface corresponds to

$$P^+(s, C_T') = \frac{P}{S\rho G^3/2} = \frac{\frac{1}{2}C_T'\rho U_d^3 A}{S\rho G^3/2} = \frac{\pi C_T'}{4s^2}\left(\frac{u_{*hi}}{G}\right)^3\left(\frac{U_d}{u_{*hi}}\right)^3 = c_{ft}'\left(\frac{u_{*hi}}{G}\right)^3\left(\frac{U_d}{u_{*hi}}\right)^3$$ (16)

where G/u_{*hi} is given by Eq. (11), and an expression for the ratio of turbine disk velocity to friction velocity, U_d/u_{*hi}, will be further addressed below.

When optimizing wind-farm power output, it may be relevant to normalize power with total cost instead of total surface area per turbine in the farm. The total cost can be divided into two parts. A first part, consists of costs which are proportionally related to the area of land used, which we will denote here with $cost_L$, expressed in units of \$/m². Elements contributing, may be the lease price of land, cost of connectivity to the power net, electric lines and civil works (e.g. in off-shore farms this is a large cost),[16] etc. A second part of the total cost, consists of costs which are proportional to the number of turbines employed, and we denote the cost per turbine with $cost_T$ [\$]. The ratio of both costs is now defined as

$$\alpha = \frac{cost_T/A}{cost_L},$$ (17)

where the turbine-rotor-disk area A is used to ensure that α is a non-dimensional constant.

Using these elements, the normalized power per unit cost is now straightforwardly defined as

$$P^*(s, C_T', \alpha) = P^+\frac{cost_L}{cost_T/S + cost_L} = P^+\frac{4s^2/\pi}{\alpha + 4s^2/\pi} = \frac{C_T'}{\alpha + 4s^2/\pi}\left(\frac{u_{*hi}}{G}\right)^3\left(\frac{U_d}{u_{*hi}}\right)^3,$$ (18)

where in a first step $cost_T$ is related to the surface area per turbine S to allow a dimensional meaningful addition of costs, and the ratio α is subsequently introduced by rearranging the equation. It is obvious that, by construction, $P^*(s, C_T', 0) = P^+(s, C_T')$.

To proceed, we will eliminate U_d/u_{*hi} from the equations by using a stream-wise momentum balance of the ABL, horizontally averaged per turbine, and integrated over its full height. The balance corresponds to

$$\int_0^H f\rho(V(z) - V_G)\ell_x\ell_y\,\mathrm{d}z = \tau_w\ell_x\ell_y + \frac{1}{2}c_{ft}'\rho U_d^3 S,$$ (19)
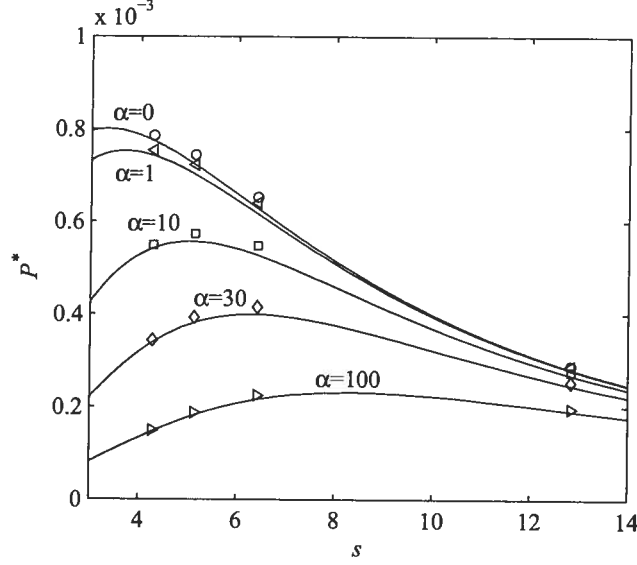
Figure 3: Normalized Power per unit cost for different values of α as function of the average turbine spacing s (and $C_T' = 4/3$). Lines: obtained from model (Eqs. 18,13,15). Symbols: from large-eddy simulations in Ref. 8, with (○): $\alpha = 0$; (◁): $\alpha = 1$; (□): $\alpha = 10$; (◊): $\alpha = 30$; and (▷): $\alpha = 100$

where $f(V(z) - V_G)$ corresponds to the driving Coriolis force in an Ekman layer,[12] and $V(z)$ is the averaged span-wise velocity as function of the height. The left-hand side of Eq. (19) corresponds to $u_{*hi}^2 \rho \ell_x \ell_y$, and also $\tau_w = \rho u_{*lo}^2$ (cf. previous subsection), such that

$$u_{*hi}^2 = u_{*lo}^2 + \frac{1}{2} c_{ft}' U_d^2. \tag{20}$$

Hence,

$$\frac{U_d}{u_{*hi}} = \left(\frac{1 - u_{*lo}^2/u_{*hi}^2}{c_{ft}'/2} \right)^{1/2}. \tag{21}$$

This equation, in combination with Eqs. (13), and (15), are now used to express U_d/u_{*hi} in Eq. (18). A combined easy-to-use analytical expression, directly expressing U_d/G (cf. Eq. 18), is provided in the Appendix, relying on an approximate solution to Eq.(11).

3. Optimal turbine spacing

Based on the formulation for the normalized power P^*, we now make an evaluation of average wind-farm power output as function of C_T', α, and s. Moreover, the optimal average turbine spacing s_{opt} is also investigated. As discussed in §2.2, we take $Ro_h = 2000$. Further, for the 'low' surface roughness we select $z_{0,lo}/z_h = 10^{-3}$ (cf. §2.3). We first focus on situations where turbines are working in optimal operating conditions, with relative high values of C_T'. This operation mode is encountered mainly in region II of a wind turbine's operation range. The effect of stalling or feathering turbines for constant power output at high wind velocities (region III of a wind turbine's operation range) on optimal turbine spacing will be briefly addressed at the end of the current section.

We first turn to the evaluation of the normalized power P^*. In Figure 3, P^* (Eq. 18) is displayed as function of s for different values of α, and $C_T' = 4/3$. The normalized power is evaluated using the

9

model proposed in the previous section, but next to that, results from the LES simulations of Calaf *et al.*[8] are also displayed. Large-eddy simulations were performed for different values of s, and C'_T: the average turbine power output P, and the induced surface roughness $z_{0,hi}$ are directly obtained from the simulations (cf. Refs. 8,9 for details on the simulation procedure, and set-up), and the respective values for P^* are obtained using Eq. (16) and (11). It is clear from Figure 3 that the model for P^* presented in the previous section, provides a reasonable fit of LES results at various average turbine spacings. Results in Figure 3 for $\alpha = 0$ show that the turbine spacing which achieves maximum power output per acre is relatively small ($s_{opt} \approx 3$). These low values (related to $s < 5$) should be interpreted with care, as the LES simulations used to construct P^* are not covering this region (cf. discussion at the beginning of Section 2.3). Moreover, when turbines are very closely spaced, turbulent fluctuations induced by the preceding row of turbines may start to reduce the effective power coefficient C'_P of the turbines, reducing the power converted to electricity (cf. Eq. 7). Further, at small distances other costs such as increased wake-turbulence induced fatigue damage and failures should be incorporated into the analysis. At higher values for α, we find that the optimum shifts to higher values of s, for which our model for P^* is better suited.

Before continuing an evaluation of the optimal turbine spacing as function of α, the effect of turbine spacing on the power output per individual turbine is highlighted in Figure 4 for three values of C'_T. In this figure, P/P_∞ is displayed as function of s, where P_∞ is the reference power output of a lone-standing turbine. It is appreciated that low values of s (< 10) significantly reduce the available power per turbine. This is a result of a lower available wind speed at hub height corresponding to a higher wind-farm induced surface roughness $z_{0,hi}$, and a slow-down of the ABL at constant geostrophic wind G. For instance, even at a relative large average spacing of $s \approx 10$, power output decreases by more then 20% compared to the power output of a lone-standing turbine. Obviously, the total farm power is also related to the number of turbines per acre (which is inversely proportional to s^2), such that optimal turbine spacings may be found at much lower values for s, as demonstrated in Figure 3.

In figure 4, we also added actual wind-farm data. To this end, we compared wind-speeds at the last row of turbines to those at the first row of turbines as obtained by the SCADA system for the Nysted and Horns Rev wind farms (reported in Frandsen et al 2007).[17] In case of the Horns Rev wind-farm, $s_x = x_y = 7$, and measurements were obtained at the 10th row of turbines, ± 5 km downstream of the first row. For the Nysted wind farms, $s_x = 10.5$, and $s_y = 5.8$. Measurements were obtained at the 8th row of turbines, ± 6 km downstream of the first row. Precise C_T (or C'_T) values are not reported. For both cases, the atmospheric boundary layer may not have reached the fully developed wind-turbine array limit, which we expect for wind-farms with horizontal extents exceeding 10–20 km. The measured data fall somewhat above the modeled normalized power in figure 4 but the agreement is reasonable given the various uncertainties involved in the analyses, measurements, and the lack of complete convergence towards a 'fully developed' limit.

The optimal turbine spacing s_{opt} is now investigated as function of α, and C'_T. In the current work, it is not our intention to provide a detailed estimation of α based on current technical and economical parameters. Instead, we will investigate a broad range of possible values for this ratio. Nevertheless, it is useful to provide at least a rough idea of what a typical value of the parameter could be. Some representative numbers that can be used are motivated as follows. For lease of land, the average yearly payout per wind turbine nowadays is around \$5,000 for present typical spacings of 500m by 500m (see e.g., *http://www.windustry.org/how-much-do-farmers-get-paid-to-host-wind-turbines*). So over a 20 year lease, this would be around $p_L \approx 0.4\$/m^2$. In some regions, the purchase of the land may be an option. For instance in Texas one may estimate a cost of \$1,000 per acre (see e.g. *http://recenter.tamu.edu/data/agp*), or approximately 0.25 \$/m^2, i.e., of similar order of magnitude to the cost of leasing. Representative cost of a wind-turbine can be found at *http://www.windustry.org/how-much-do-wind-turbines-cost*. The average cost is listed as \$3.5×10^{6}
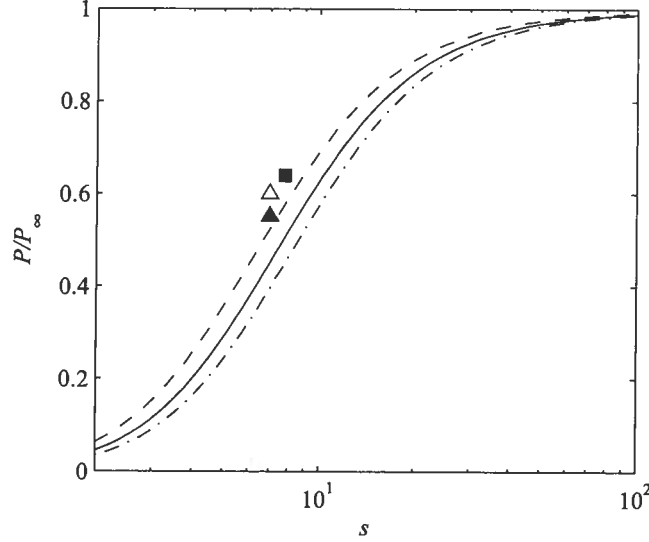
Figure 4: Power output per turbine as function of turbine spacing s, normalized with power output of a lone-standing turbine. (—−) $C_T' = 1.0$; (—) $C_T' = 4/3$; (−·) $C_T' = 5/3$. Symbols represent wind-farm measurements. ($\triangle$,$\blacktriangle$): Horns Rev wind farm ($s = 7$), last row compared to front row (west–east) at measured respectively 8.5 and 12.5 m/s of wind speed (cf. Ref. 17, 18); ($\blacksquare$): Nysted wind farm ($s^2 = 10.5 \times 5.8$), last row compared to front row (west–east) measured with 8.5 m/s of wind speed (cf. Ref. 17).

for a 2MW rated wind turbine. Using a representative turbine diameter of 70m one arrives at a cost factor per square diameter of $cost_T \approx 700\$/m^2$. The corresponding parameter α is then roughly in the range of $1.5 - 3 \times 10^3$. In the current work, we will cover a range of values for α from $\alpha = 0$ (corresponding to no costs per turbine) to $\alpha = 10^4$.

In Figure 5 the optimal turbine spacing s_{opt} is displayed as function of α. By investigating various values of α and C_T', we found that only one global optimum exist for a given value of α, and C_T' (see, e.g., Figure 3). The farm-power model provided in the previous section was implemented in MATLAB, and for the optimization, we employ the *fminbnd* function with bounds $0 \leq s \leq 40$. This method combines standard optimization algorithms, such as parabolic interpolation, and golden section search (cf., e.g, Ref. 19).

In Figure 5(a), the optimal spacing is given for three values of C_T'. It is clear that α has a strong influence on s_{opt}, with optimal values ranging from $s \approx 4$ for $\alpha = 1$ to $s \approx 25$ for $\alpha = 10^4$. An analysis of the trends at large α suggests a scaling behavior of $s_{opt} \sim \alpha^{1/4}$, in the limit $\alpha \to \infty$. Obviously, for low values of α and low values of s_{opt}, other factors may play a decisive role in the selection of the average turbine spacing in wind farms (such as, e.g., constraints imposed by fatigue loading in closely placed turbines). For large values of α (e.g. $10^3 < \alpha < 10^4$, which may be economically more relevant), it is appreciated that optimal turbine spacing is larger than $s_{opt} \approx 15$. This is considerably larger than typical average spacings currently used in large wind farms both on and off shore (e.g., the well known Horns Rev wind farm off the coast of Denmark, has an average farm spacing of $s = 7$).

In order to investigate the sensitivity of the optimal farm power output P^* to variations of s around the optimum s_{opt}, we evaluated sub-optimal solutions in Figure 5(b). To this end, we define the suboptimal spacing $s_\eta(\alpha)$ as the spacing that gives a power output of $P^*[s = s_\eta(\alpha)] = \eta P^*_{opt}$ (and $s < s_{opt}$). Hence $s_x(\alpha)$ provides a spacing which is lower then s_{opt}, and has a power efficiency of
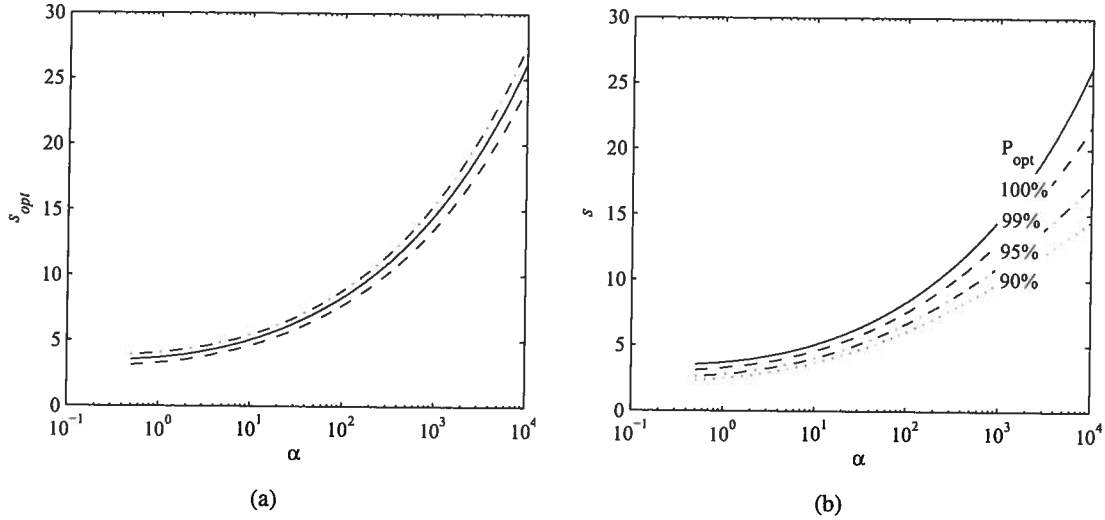
11

Figure 5: (a) Optimal turbine spacing s_{opt} as function of the ratio α for different values of C_T': (—) $C_T' = 1.0$; (—) $C_T' = 4/3$; and (-·) $C_T' = 5/3$. (b) Smallest turbine spacing as function of α (and for $C_T' = 4/3$) for which the normalized power output P^* corresponds with (—) $100\% P^*_{opt}$; (--) 99% of P^*_{opt}; (-·) 95% of P^*_{opt}; and (·· ·) 90% of P^*_{opt}

η compared to the power at optimal spacing. In Figure 5(b), results are shown for $s_{99\%}$, $s_{95\%}$, $s_{90\%}$, together with s_{opt}. Especially at high values of α, it is appreciated that a reduction in desired overall farm–ABL efficiency allows to reduce the spacing significantly. For instance, taking $\alpha = 10^4$, and $\eta = 95\%$ allows to reduce the optimal spacing $s_{opt} \approx 25$ to a spacing of $s \approx 15$.

Finally we turn our attention to region III operation of wind turbines where turbine-power output is limited to a constant value, independent of wind speed, by pitching the turbine blades, either to feather or to stall the turbine.[4] In the case of pitching to feather, the angle of attack of the turbine blades is decreased such that the lift forces decrease. In this case the thrust forces decrease, while, since the flow remains attached in this regime, the ratio C_P'/C_T' remains constant. In the case of pitching to stall, the angle of attack of the turbine blades is increased, such that the turbine starts to stall. In this case, the ratio C_P'/C_T' decreases, but the thrust force and the thrust coefficient C_T' does not decrease, and may initially even increase. Obviously, the different behavior of C_T' in both control methods, may differently affect the wind-farm ABL interaction.

In practice, wind-farm optimization of P^* should be performed over the whole operating region of the turbine, weighted with statistical distribution of geostrophic wind speeds available at a certain location (e.g. assuming a classical Weibull distribution to characterize the wind-speed probability density function).[10] In case power in region III operation is controlled by stalling the turbine, the optimal turbine spacing will not differ significantly from the results presented above for region II operation. In this case, C_P'/C_T' is modulated by stalling the turbine blades, but C_T' remains roughly constant, close to its region II value. Hence, the control in region III does not affect the wind-farm–ABL interaction.

Region III operation becomes quite different when turbines are feathered to control the power output to a constant. In this case, C_P'/C_T' is kept constant, and C_T' decreases by reducing the angle of attack of the turbine blades. As a result, the ABL partially speeds up. In Figure 6(a), this situation is demonstrated for different values of α, and starting with a region-II value of $C_T' = 4/3$, and a turbine spacing $s_{ref} = s_{opt}$ which is optimally designed for region II operation. The figure shows the power output P^+ normalized with the power output P^+_{ref} at $C_T' = 4/3$. Especially for low values of α (for
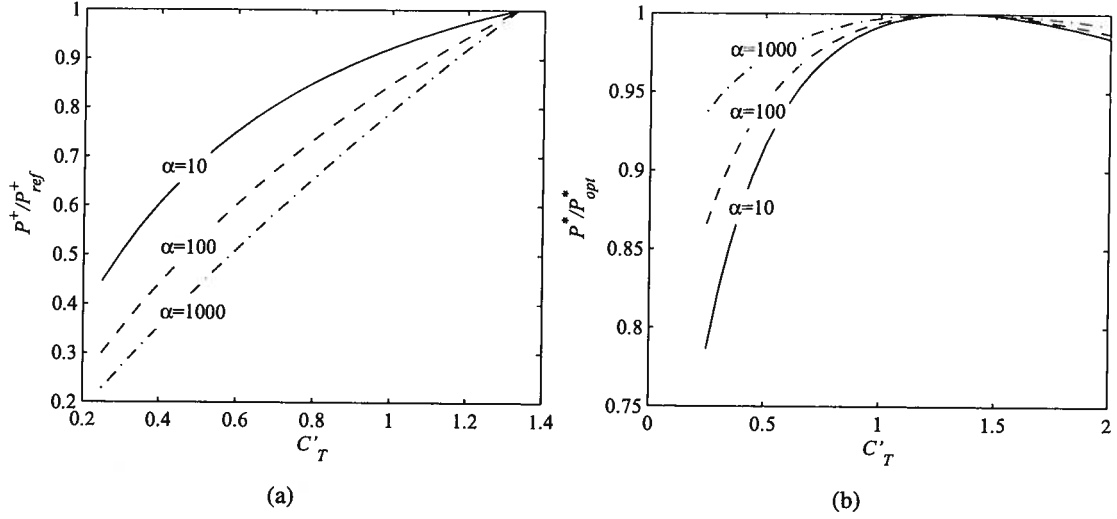
Figure 6: (a) Ratio of $P^+(s_{ref}, C_T')$ to $P_{ref}^+(s_{ref}, 4/3)$ (with $s_{ref} = s_{opt}(C_T'=4/3)$, the optimal value for $C_T' = 4/3$) as function of the thrust coefficient C_T'. (b) Dependence of $P^*(s_{ref}, C_T')/P_{opt}^*(s_{opt}, C_T')$ on C_T', with $s_{ref} = s_{opt}(C_T'=4/3)$.

which s_{opt} is low, cf. Figure 5) we find a large influence of the wind-farm–ABL interaction on the control. For lone-standing turbines, we would expect P^+ to decrease linearly with C_T'. Instead, for low values of α, a decrease of C_T' leads to an acceleration of the ABL, such that P^+ decreases less then linearly. For high values of α this effect diminishes, since here s_{opt} is higher, approaching more and more the situation of lone-standing turbines.

Since feathering turbines in region III affects the ABL, this will also reflect on the optimal wind-turbine spacing in wind farms, which may differ from the optimal obtained for region-II operation (in contrast to stalling the turbines). To further illustrate this, Figure 6(b) shows the ratio $P^*(s_{ref}, C_T')/P_{opt}^*(s_{opt}, C_T')$ as function of C_T', where $P^*(s_{ref}, C_T')$ is the normalized power output of a farm with spacing s_{ref} designed to be optimal at an operational point with $C_T' = 4/3$, while $P_{opt}^*(s_{opt}, C_T')$ is the normalized power output for a farm designed to be optimal for C_T'. When C_T' is decreased (starting from $C_T' = 4/3$) it is appreciated that the ratio of P^* to the optimal value decreases, as the turbine spacing s_{ref} is not optimal for these lower values of C_T'. Optimizing P^* for the whole operation range of the turbines in a wind farm is then equivalent to optimization with on average lower C_T' values, leading to lower turbine spacings (cf. also Figure 5).

4. CONCLUSIONS

Following a recent computational study of very large wind farms, in which a new parametrization of effective roughness height was proposed,[8] we explored in the current work implications on optimal spacing among wind turbines. The limit of "infinite wind farms", when the overlaying atmospheric boundary layer has become "fully developed", is relevant in practice for wind farms on flat terrain whose length exceeds the height of the atmospheric boundary layer by over an order of magnitude. Then the boundary layer has reached a new constant equilibrium height and turbulence levels no longer change with downstream direction. In this limit the power extraction is dominated by vertical entrainment of kinetic energy.[8,15] For optimal wind turbine spacing, the figure of merit that has been used here is the total power extracted for a given geostrophic wind velocity. Depending on the ratio

13

of land-surface costs and turbine costs, different optimal spacings have been obtained. For realistic cost ratios, we find that the optimal average turbine spacing may be considerably higher ($\sim 15D$) then conventionally used in current wind-farm implementations ($\sim 7D$).

Naturally, the conclusions reached here are subject to considerable limitations. The approach is based on parameterizations of wind-farm–ABL interactions under neutral stratification conditions, and assumes a flat terrain with no topography. Very often, for land-based wind farms the topography will locally affect the interactions and thus affect the optimal arrangement. For large offshore wind farms, the distribution of costs according to 'per-turbine' or 'per surface area' may be more difficult to specify and depend greatly on conditions of connectivity, typical sea states, distances to the coast, etc. It is also important to point out that the current findings are relevant to optimal spacing in the "fully developed wind turbine array boundary layer" for wind farms that are significantly larger than the fetch required for a surface disturbance to reach equilibrium with the entire ABL. Normally this is assumed to take about 10 times the height of the ABL, i.e. we may consider the present analysis to be relevant for wind farms larger than (say) 10 km. For shorter wind farms, the optimal spacing may depend on location, as the front wind turbines will be operating under more powerful incoming winds.

Finally, the parametrization makes no distinction among span-wise and stream-wise spacings of wind turbines, or effects of staggering their locations (or considering a tilted inflow). As shown (e.g.) in LES,[9] increases on the order of 5% can be expected in the extracted power when one staggers the turbines. The overall optimization trends as predicted here will vary slightly under such conditions, but we expect the major trends to be the same. Still, especially in locations with strong prevailing wind directions in which staggering can be an important part of the optimization, differences with present predictions may be expected. More accurate optimization and prediction of the optimal power for large wind farms (in which the detailed couplings with the ABL are crucial) will need to await more generally valid and accurate parameterizations of wind-turbine–ABL interactions. This should include effects of thermal stratification, wind turbine arrangements, and complex terrain.

Acknowledgments

APPENDIX

In the current work, we rely partially on relations with an implicit formulation (e.g. Eq. 11), which we solve numerically by means of an iterative solver (cf. §2.2). Here we present an easy-to-use alternative expression, which allows to evaluate U_d/G (required to obtain the normalized power) directly, by using an approximation for Eq. (11). We begin by using an approximate fit to the solution of Eq. (11) similar to that used before:[7,20]

$$\frac{G}{u_{*hi}} \approx \frac{1}{\kappa}\left(\ln Ro - A_*\right). \tag{22}$$

The parameter A_* is a fitting parameter which depends on Ro. For $10^4 < Ro < 9 \times 10^5$, we find $A_* \approx 3.2$, with a maximum relative error of 7% on the prediction of G/u_{*hi} (this range for Ro corresponds with $Ro_h = 2000$, $C_T' = 4/3$, and $25 > s > 3$ encountered in the current work).

Using the model expression for $z_{0,hi}/z_h$ (Eq. 15) in the approximation yields

$$\frac{G}{u_{*hi}} \approx \frac{V_w}{\sqrt{1 + c_{ft}V_w^2/2}} + \frac{1}{\kappa}\left(\ln\left[Ro_h\left(1 + \frac{D}{2z_h}\right)^{\frac{-v_w^*}{1+v_w^*}}\right] - A_*\right) \tag{23}$$

where V_w is a dimensionless velocity given by the expression

$$V_w = \frac{1}{\kappa}\ln\left[\frac{z_h}{z_{0,lo}}\left(1 - \frac{D}{2z_h}\right)^{\frac{v_w^*}{1+v_w^*}}\right] \tag{24}$$

(the velocity V_w may be understood as an extrapolation from below the turbine wake of the average wind-farm velocity at farm hub height).[8] The wake viscosity v_w^* is given by Eq. (14) ($v_w^* \approx 28\sqrt{c_{ft}/2}$), $c_{ft} = \pi C_T/4s^2$ and c_{ft}/c_{ft}' depends upon the operating region (as described in the main text, for region II we use $c_{ft}/c_{ft}' = 9/16$). Starting from Eq. (21), the ratio of disk velocity to friction velocity, also needed in Eq. (18), can be simplified to read

$$\frac{U_d}{u_{*hi}} = \frac{V_w\sqrt{c_{ft}/c_{ft}'}}{\sqrt{1 + c_{ft}V_w^2/2}}. \tag{25}$$

Summarizing and further simplifying, the overall ratio U_d/G required in Eq. (16) can be written as

$$\frac{U_d}{G} = \sqrt{\frac{c_{ft}}{c_{ft}'}}\left[1 + \frac{\sqrt{1 + \frac{c_{ft}}{2}V_w^2}}{\kappa V_w}\left(\ln\left[Ro_h\left(1 + \frac{D}{2z_h}\right)^{\frac{-v_w^*}{1+v_w^*}}\right] - A_*\right)\right]^{-1} \tag{26}$$

Equation (26) provides an estimate of U_d/G with a maximum relative error of 7% due to the approximation in Eq. (22) (using $A_* = 3.2$). The expression should be handled with care when evaluating the normalized farm power (Eqs. 16,18), which depends on $(U_d/G)^3$. Using the approximate fit of Eq. (26), this yields a maximum relative error of about 20%. This is the reason that in the current work, we selected not to use the approximation in Eq. (22), as discussed above (see also §2.2). Nevertheless, since relative trends will be reasonably well predicted it is still useful to have such simplified expressions available for more qualitative parameter explorations.

References

1. US Department of Energy. 20% wind energy by 2030: Increasing wind energy's contribution to U.S. electricity supply, 2008.

2. Commission of the European Communities. A European strategic energy technology plan – technology map, 2007.

3. Snel H. Review of the present status of rotor aerodynamics. *Wind Energy* 1998; **1** : 46–49.

4. Burton T, Sharpe D, Jenkins N, Bossanyi E. *Wind Energy Handbook*. John Wiley & Sons: New York, 2001.

5. Vermeer LJ, Sorensen JN, Crespo A. Wind turbine wake aerodynamics. *Progress in Aerospace Sciences* 2003; **39** : 467–510.

15

6. Frandsen S. On the wind speed reduction in the center of large clusters of wind turbines. *J. Wind Eng Indust. Aerodyn.* 1992; **39** : 251–265.

7. Frandsen S, Barthelmie R, Pryor S, Rathmann O, Larsen S, Højstrup J, Thøgersen M. Analytical modelling of wind speed deficit in large offshore wind farms. *Wind Energy* 2006; **9** : 39–53.

8. Calaf M, Meneveau C, Meyers J. Large eddy simulation study of fully developed wind-turbine array boundary layers. *Physics of Fluids* 2010; **22** : Art no 015110. DOI:10.1063/1.3291077

9. Meyers J, Meneveau C. Large eddy simulations of large wind-turbine arrays in the atmospheric boundary layer. In *48th AIAA Aerospace Sciences Meeting Including the New Horizons Forum and Aerospace Exposition*, January 2010. Art no AIAA2010-827.

10. Manwell JF, McGowan JG, Rogers AL Wind Energy Explained: Theory, Design and Application Wiley, 2002.

11. Jimenez A, Crespo A, Migoya E, Garcia J Advances in large-eddy simulation of a wind turbine wake. *J. of Physics: Conference Series*, 2007, **75** : 012041.

12. Tennekes H, Lumley JL. *A first Course in Turbulence*. The MIT Press, 1972.

13. Castro IP. Rough-wall boundary layers: mean flow universality. *Journal of Fluid Mechanics* 2007; **585** : 469–284.

14. Wu Y-T, Porté-Agel F. Large-Eddy Simulation of Wind-Turbine Wakes: Evaluation of Turbine Parameterizations. *Boundary-Layer Meteorology*, DOI 10.1007/s10546-010-9569-x, published online December 2010.

15. Cal RB, Lebrón J, Castillo L, Kang HS, Meneveau C. Experimental study of the horizontally averaged flow structure in a model wind-turbine array boundary layer. *J. Renewable Sustainable Energy* 2010; **2** : Art no 013106. DOI:10.1063/1.3289735

16. Fuglsang P, Thomsen K. Cost optimization of wind turbines for large-scale off-shore wind farms. Technical Report Risø-R-1000(EN), Risø National Laboratory, Roskilde, Denmark, 1998.

17. Frandsen S, Barthelmie R, Rathmann O, Jørgensen HE, Badger J, Hansen K, Ott S, Rethore P-E, Larsen SE, Jensen LE The shadow effect of large wind farms: measurements, data analysis and modelling. Technical Report Risø-R-1615, Risø National Laboratory, Roskilde, Denmark, 2007

18. Barthelmie RJ, Rathmann O, Frandsen ST, Hansen K, Politis E, Prospathopoulos J, Rados K, Cabezón D, Schlez W, Phillips J, Neubert A, Schepers JG, van der Pijl SP Modelling and measurements of wakes in large wind farms Journal of Physics: Conference Series 2007; **75**: Art no 012049.

19. Brent RP. *Algorithms for Minimization without Derivatives*. Prentice-Hall: Englewood Cliffs, New Jersey, 1973.

20. Emeis S, Frandsen S. Reduction of horizontal wind speed in a boundary layer with obstacles. *Boundary-Layer Meteorology* 1993; **64** : 297–305.

NREL
NATIONAL RENEWABLE ENERGY LABORATORY

NREL HOME

ABOUT NREL | ENERGY ANALYSIS | SCIENCE & TECHNOLOGY | TECHNOLOGY TRANSFER | APPLYING TECHNOLOGIES

‖More Search Options   Search
‖Site Map

■ FEATURED LINKS

‹ Data Book Home

Table of Contents

Browse by Technology

Calculators

  Renewable Energy Conversion

  Photovoltaic Land Area

  Wind Power Land Area

  Energy Growth Estimator

Archives

Contact Us

Wind Farm Area Calculator

This calculator estimates land-area requirements for wind power systems. The results indicate a "footprint" of land that has to be taken out of production to provide space for turbine towers, roads, and support structures.

The "footprint," which is typically around 0.25 acres per turbine, does not include the 5-10 turbine diameters of spacing required between wind turbines. Because of this spacing, the area included within the perimeter of the wind farm will be larger. However, it is important to note that the land between the turbines - minus the "footprint" area - is still usable for its original purpose. For a more detailed analysis of land use by wind farms, please see Land-Use Requirements of Modern Wind Power Plants in the United States.

Biomass Energy Data Book

Buildings Energy Data Book

Hydrogen Energy Data Book

Transportation Energy Data Book

■ FEATURES

SEAC   Strategic Energy Analysis Center

Energy Analysis Newsletter ▶

Input Value	1000	(kW)
Area per turbine	0.25	(Acres)
Size of turbine	1000	(kW)

submit

The estimated land area required is: **0.25 acres**.
This calculation assumes **1"000 kW** and **1 turbines** each requiring an area of **0.25 acres**.
Note: This value represents the area taken out of production on a farm.
The area within the perimeter of the wind farm will be larger due to spacing of the turbines, but is still useable by the farm.
Typical turbine spacing in wind farms is placing the towers 5 to 10 turbine diameters apart, depending on local conditions.

Printable Version

Webmaster | Security & Privacy | Disclaimer | NREL Home

| TECHNOLOGY | GRID INTEGRATION | ECONOMICS | INDUSTRY & MARKETS | ENVIRONMENT | SCENARIOS & TARGETS |

Search : [OK]

Home

Executive Summary

Factsheets

Myths

Satisfaction questionnaire

MAIN PUBLICATION :

Technology

Introduction

Wind resource estimation

Wind Turbine Technology

Wind farm design

Offshore

Small Wind Turbines

Research and Development

APPENDIX

ABREVIATIONS

GLOSSARY

REFERENCES

EVENTS

Downloads

How to order?

Home » TECHNOLOGY » Wind farm design » Factors affecting turbine location » Turbine loads

Turbine Loads

A key element of the layout design is the minimum turbine spacing used. In order to ensure that the turbines are not being used outside their design conditions, the minimum acceptable turbine spacing should be obtained from the turbine supplier and adhered to.

The appropriate spacing for turbines is strongly dependent on the nature of the terrain and the wind rose for a site. If turbines are spaced closer than 5 rotor diameters (5D) in a frequent wind direction, it is likely that unacceptably high wake losses will result. For areas with predominantly unidirectional wind roses, such as the San Gorgonio Pass in California, or bi-directional wind roses, such as Galicia in Spain, greater distances between turbines in the prevailing wind direction and tighter spacing perpendicular to the prevailing wind direction will prove to be more productive.

Tight spacing means that turbines are more affected by turbulence from the wakes of upstream turbines. This will create high mechanical loads and requires approval by the turbine supplier if warranty arrangements are not to be affected.

Separately from the issue of turbine spacing, turbine loads are also affected by:

- 'Natural' turbulence caused by obstructions, topography, surface roughness and thermal effects; and
- Extreme winds

Defining reliable values for these parameters, for all turbine locations on the site, may be difficult. Lack of knowledge is likely to lead to conservative assumptions and conservative design.

Within the wind industry there is an expectation that all commercial wind turbines will be subject to independent certification in accordance with established standards or rules. A project-specific verification of the suitability of the certification for the proposed site should be carried out, taking into account the turbine design specifications and the expected climatic conditions of the site.

<< Noise

Acknowledgements | Sitemap | Partners | Disclaimer | Contact

coordinated by

EWEA

supported by

Intelligent Energy
Europe

Website by Easy-Concept

For immediate release:
Feb. 26, 2008

For more information:
Lisa Morawski, 503-947-7897,
lisa.m.morawski@state.or.us

Oregon OSHA releases findings in wind turbine collapse
State fines Siemens Power Generation for the fatal incident

(Salem) — The Oregon Department of Consumer and Business Services, Occupational Safety and Health Division (Oregon OSHA) has fined Siemens Power Generation Inc. a total of $10,500 for safety violations related to an Aug. 25, 2007 wind turbine tower collapse that killed one worker and injured another.

"The investigation found no structural problems with the tower," said Michael Wood, Oregon OSHA administrator. "This tragedy was the result of a system that allowed the operator to restart the turbine after service while the blades were locked in a hazardous position. Siemens has made changes to the tower's engineering controls to ensure it does not happen again."

The event took place at the Klondike III Wind Farm near Wasco, where three wind technicians were performing maintenance on a wind turbine tower. After applying a service brake to stop the blades from moving, one of the workers entered the hub of the turbine. He then positioned all three blades to the maximum wind resistance position and closed all three energy isolation devices on the blades. The devices are designed to control the mechanism that directs the blade pitch so that workers don't get injured while they are working in the hub. Before leaving the confined space, the worker did not return the energy isolation devices to the operational position. As a result, when he released the service brake, wind energy on the out-of-position blades caused an "overspeed" condition, causing one of the blades to strike the tower and the tower to collapse, the Oregon OSHA investigation found.

Chadd Mitchell, who was working at the top of the tower, died in the collapse. William Trossen, who was on his way down a ladder in the tower when it collapsed, was injured. The third worker was outside the tower and unharmed.

During the investigation, Oregon OSHA found several violations of safety rules:

- Workers were not properly instructed and supervised in the safe operation of machinery, tools, equipment, process, or practice they were authorized to use or apply. The technicians working on the turbine each had less than two months' experience, and there was no supervisor on site. The workers were unaware of the potential for catastrophic failure of the turbine that could occur as a result of not restoring energy isolation devices to the operational position.

- The company's procedures for controlling potentially hazardous energy during service or maintenance activities did not fully comply with Oregon OSHA regulations. Oregon OSHA requirements include developing, documenting, and using detailed procedures and applying lockout or tagout devices to secure hazardous energy in a "safe" or "off" position during service or maintenance. Several energy isolation devices in the towers, such as valves and lock pins, were not designed to hold a lockout device, and energy control procedures in place at the time of the accident did not include the application and removal of tagout devices.

- Employees who were required to enter the hub (a permit-required confined space) or act as attendants to employees entering the hub had not been trained in emergency rescue procedures from the hub.

Siemens Power Generation has 30 days to appeal the citation.

###

Oregon OSHA, a division of the Department of Consumer & Business Services, enforces the state's workplace safety and health rules and works to improve workplace safety and health for all Oregon workers. For more information, go to www.orosha.org.

The Department of Consumer and Business Services is Oregon's largest business regulatory and consumer protection agency. For more information, visit www.dcbs.oregon.gov.